Exosomes secreted by endothelial cells derived from human induced pluripotent stem cells protect heart from myocardial infarction by modulating cardiomyocyte calcium homeostasis

hao li
Tongji University
lu wang
Tongji University
teng ma
Tongji University
zhongming liu
Tongji University
ling gao (gaoleng5@126.com)
Tongji University https://orcid.org/0000-0002-6391-6724

Research Article

Keywords: hiPSC-ECs, exosomes, Ca2+ homeostasis, miR-100-5p

Posted Date: July 14th, 2022

DOI: https://doi.org/10.21203/rs.3.rs-1837561/v1

Exosomes secreted by endothelial cells derived from human induced pluripotent stem cells protect heart from myocardial infarction by modulating cardiomyocyte calcium homeostasis

Hao Li[1], Lu Wang[1], Teng Ma[1], Zhongmin Liu[1,2,3,4*], Ling Gao[1,3,4*]

1. Translational Medical Center for Stem Cell Therapy & Institutes for Regenerative Medicine, Shanghai East Hospital, Tongji University School of Medicine, Shanghai 200123, China.
2. Department of Cardiovascular and Thoracic Surgery, Shanghai East Hospital, Tongji University School of Medicine, Shanghai 200120, China.
3. Shanghai Institute of Stem Cell Research and Clinical translation, Shanghai East Hospital, Tongji University, Shanghai 200120, China.
4. Shanghai Engineering Research Center for Stem Cell Clinical Treatment, Shanghai 200123, China.

*Addresses for correspondence

Ling Gao, PhD
Translational Medical Center for Stem Cell Therapy & Institute for Regenerative Medicine, Shanghai East Hospital, Tongji University School of Medicine, 1800 Yuntai Rd., Shanghai, 200123, China;
E-mail: gaoleng5@126.com

Zhongmin Liu, MD, PhD
Department of Cardiovascular and Thoracic Surgery, Shanghai East Hospital, Tongji University School of Medicine, 150 Jimo Rd., Shanghai, 200120, China;
E-mail: liu.zhongmin@tongji.edu.cn

Abstract

Background: Human induced pluripotent stem cell–derived endothelial cells (hiPSC-ECs) exhibit potential in repairing the injured heart after myocardial infarction (MI) by promoting neovascularization and cardiomyocyte survival. However, because of the low cellular retention and poor engraftment efficacy, cell therapy treatment of MI is in part mediated by exosomes secreted from the transplanted cells. We investigated whether exosomes secreted from hiPSC-ECs could become a promising acellular approach to repairing the infarcted heart after MI, and elucidated the underlying protective mechanism.

Methods: hiPSC-ECs were differentiated and exosomes were isolated in vitro. Then, hiPSC-EC exosomes were delivered by intramyocardial injection in a murine MI model in vivo. Echocardiography, combined with hemodynamic measurement, histological examination, Ca^{2+} transient and cell shortening assessment, and western blot, was used to determine protective effects of hiPSC-EC exosomes on the infarcted heart. Furthermore, microRNA sequencing, luciferase activity assay, and microRNA gain–loss function experiments were performed to investigate the enriched microRNA and its role in exosome-mediated effects.

Results: In vitro assessments demonstrated that hiPSC-EC exosomes could be taken up by cardiomyocytes and that they possess the capability to protect cardiomyocytes from oxygen–glucose deprivation injury by enhancing Ca^{2+} transients, increasing ATP content, and promoting cell survival. Congruously, hiPSC-EC exosomes administration in vivo not only improved myocardial contractile function but also attenuated the harmful left ventricular remodeling after MI. Mechanistically, hiPSC-EC exosomes notably rescued the protein expression and function of sarcoplasmic reticulum Ca^{2+} ATPase 2a (SERCA-2a) and ryanodine receptor 2 (RyR-2) to maintain intracellular Ca^{2+} homeostasis and increase cardiomyocyte contraction after MI. microRNA sequencing determined that miR-100-5p was the most abundant microRNA in exosomes, and miR-100-5p could target protein phosphatase 1β (PP-1β) to enhance the phosphorylation level of phospholamban (PLB) at Ser^{16} and subsequent SERCA activity, which contributes to the hiPSC-EC exosome–exerted cytoprotective effects on maintaining intracellular Ca^{2+} homeostasis and promoting cardiomyocyte survival.

Conclusion: hiPSC-EC exosomes maintain cardiomyocyte Ca^{2+} homeostasis to improve myocardial recovery after MI, which may provide an acellular therapeutic option for myocardial injury.

Keywords: hiPSC-ECs, exosomes, Ca^{2+} homeostasis, miR-100-5p

Introduction

Myocardial infarction (MI), which contributes to irreversible cell death and subsequent heart failure, is a leading cause of morbidity and mortality worldwide [1-4]. Cell therapy, such as human induced pluripotent stem cell–derived endothelial cells (hiPSC-ECs), has emerged as a potential approach to repairing the infarcted heart [5, 6]. There is convincing evidence that iPSC-ECs (human and swine origin) could act as a regenerative cargo to protect the heart against ischemic injury by promoting neovascularization and cardiomyocyte survival [5-7]. However, low cellular retention and poor engraftment efficacy limit the therapeutic potential of iPSC-ECs and indicate that paracrine signaling is the fundamental mechanism of the promising cardioprotective effects mediated by iPSC-ECs [7]. Exosomes are soluble factors released by the transplanted cells and may provide an alternative approach for ischemic diseases [8, 9]. Therefore, it is interesting to investigate whether hiPSC-EC exosomes could become a novel acellular option to promote the infarcted heart healing after MI, and to elucidate the underlying mechanism.

Defects of Ca^{2+} homeostasis are a critical hallmark of a failing heart because cardiomyocyte function depends on synchronized movements of Ca^{2+} cycling, which contributes to the heart rhythm and excitation–contraction coupling. There is cumulative evidence showing gross Ca^{2+} homeostasis disorders after MI, such as decreased Ca^{2+} transients, reduced sarcoplasmic reticulum (SR) Ca^{2+} content, and diminished SR Ca^{2+} uptake and sequestration. These abnormalities are attributed to the expression and function alterations of Ca^{2+}-handling proteins and transporters. Ryanodine receptor 2 (RyR-2), which results in releasing Ca^{2+} from SR, could be a potential therapeutic target in MI [10]. Numerous findings have raised the possibility that the dysfunction of RyR-2 induced by oxidative stress during heart failure (HF) could contribute to both SR content and Ca^{2+} transient reduction because the channels cannot close during the diastole [11]. Moreover, SR Ca^{2+} ATPase 2a (SERCA-2a), which pumps Ca^{2+} back into SR, and Na^{+}/Ca^{2+} exchange 1 (NCX-1), which transports Ca^{2+} out of the cell, have synergistic or antithetic effects to remove Ca^{2+} from the cytosol [12, 13]. Collectively, both SERCA-2a and NCX-1 functions could be impaired as a consequence of either expression inhibition or function depression after MI, which might contribute to Ca^{2+} overload in cytosol and cardiac dysfunction [12, 13]. Hence, modulating Ca^{2+} homeostasis might be a potential therapeutic approach toward MI. However, it is elusive whether hiPSC-EC exosomes could maintain intracellular Ca^{2+} homeostasis and promote cardiomyocytes survival to ameliorate infarcted heart function and reduce harmful remodeling, and the underlying mechanism needs to be

further explored. Moreover, considering that microRNAs are one of the most active ingredients contained in exosomes [14-16], there is also a strong rationale to elucidate which microRNA contained in hiPSC-EC exosomes is the decisive factor to regulate Ca^{2+} homeostasis and protect cardiomyocytes from ischemic injury.

Therefore, in this study, we extracted exosomes from hiPSC-ECs and identified their characteristics. Then, combining in vitro and in vivo strategy, we investigated (i) whether hiPSC-EC exosome administration could promote cardiomyocyte survival and repair the infarcted heart after MI; (ii) whether hiPSC-EC exosomes could modulate intracellular Ca^{2+} homeostasis to protect resident cardiomyocytes; (iii) which microRNA is the most abundant ingredient and mainly contributes to hiPSC-EC exosome–mediated beneficial effects; and (iv) the underlying mechanisms.

Methods:

hiPSC-EC generation and characterization

hiPSCs used in this study were reprogrammed from human umbilical cord blood mononuclear cells via transduction of OCT4, SOX2, KLF4, and cMYC. Differentiation of endothelial cells was carried out as previously reported [17]. Then, hiPSC-ECs were enriched to >95% by flow-cytometry selection for both CD31 and CD144 expression. The differentiated hiPSC-ECs were characterized via immunofluorescent staining of CD31, CD144, and von Willebrand factor (VWF), and their purity was analyzed by flow cytometry. Tube formation was evaluated as previously reported [18]. The Dil-conjugated acetylated low-density lipoprotein (Ac-LDL) uptake assay was also conducted as described previously [18].

hiPSC-EC exosome isolation and identification

hiPSC-EC–secreted exosomes (EC-Exo) were purified from culture medium using an ExoQuick^{TM} Precipitation Solution Kit (SBI, USA) as described previously [19, 20]. Particle size distributions and yield of exosomes reconstituted in phosphate buffered saline (PBS) were determined by nanoparticle tracking analysis with NanoSight. Protein content was measured via MicroBCA Protein Assay Kit (Beyotime, China), and the expression levels of exosomal marker proteins (ALG-2-interacting protein X [Alix], tumor susceptibility gene 101 protein [TSG101], CD63, CD9) were evaluated by western blot. The ultrastructure of exosomes was evaluated via transmission electron microscopy as described previously [6]. Congruously, miR-100-5p inhibitor (100 nM) oligonucleotides or negative control (NC) oligonucleotides (RiboBio, China) were transfected into hiPSC-ECs by using Ribo FECT^{TM} CP Transfection Kit (RiboBio). Then, exosomes secreted by the transfected hiPSC-ECs were isolated and identified as EC-Exo$^{anti\text{-}miR\text{-}100\text{-}5p}$ or EC-Exo^{NC}.

Exosome uptake assessment

hiPSCs were differentiated into cardiomyocytes (hiPSC-CMs) as previously reported [6]. In order to monitor the internalization of hiPSC-EC exosomes, the purified hiPSC-EC exosomes were labeled with a PKH26 Red Fluorescent Cell Linker Kit (Sigma-Aldrich, USA) for in vitro studies in accordance with the manufacturer's instructions. Then, the prelabeled exosomes were added to hiPSC-CMs, which were subsequently fixed and immunofluorescently stained.

In vitro exosome cytoprotection assay

hiPSC-CMs were seeded into 24-well plates or four-chamber slides (BioLogix, China), and separately treated with PBS, EC-Exo (1 μg/mL), EC-Exo^{NC} (1 μg/mL), EC-Exo$^{anti\text{-}miR\text{-}100\text{-}5p}$ (1 μg/mL), mimic NC (100 nM), and miR-100-5p mimic (100 nM). Mimic NC and miR-100-5p mimic were transfected using Lipofectamine RNAi$_{MAX}$ Kit (Thermo Fisher Scientific, USA). Then, cardiomyocytes were cultured under normal or oxygen–glucose deprivation condition (glucose-free DMEM without serum, 1% O_2/5% CO_2/94% N_2) for 48 hours. Apoptosis was evaluated with an In Situ Cell Death Detection Kit (Roche Applied Science, Germany). Lactate dehydrogenase (LDH) leakage in the culture medium was determined with a CytoTox-One homogenous membrane integrity assay (Promega, USA). ATP content was measured in homogenized hiPSC-CMs using ATP Bioluminescence Assay Kit (Sigma-Aldrich). Ca^{2+} transients were evaluated by incubating hiPSC-CMs with a Ca^{2+} indicator, Fura-2 AM (Yeasen, China), and electrically stimulating the cells. Then, the ratio of fluorescence emitted at 340 nm and 380 nm was recorded using a Ca^{2+}-recording system (IonOptix, USA) [21].

Murine model of MI

MI was produced in NOD-Prkdc^{scid} Il2rg^{em1}/Smoc mice (M-NSG, Shanghai Model Organisms Center, China), aged between 8 and 12 weeks, by permanently ligating the left anterior descending (LAD) coronary artery [19]. Animals in the MI+EC-Exo group received hiPSC-EC exosomes (20 μg in 20 μL PBS) by intramyocardial injection to three sites in the anterior wall of the left ventricle (LV); animals in the MI group received 20 μL PBS by intramyocardial injection; and animals in the Sham group underwent all surgical procedures for MI induction, except for occlusion, and recovered without any of the experimental treatments. At the end of the experiment, the hearts were collected and cut in half; one half was used for histological analyses, and the other half was used for protein extraction.

Echocardiography

Echocardiography was performed on a Vevo 2100 Imaging System (Visual Sonics Inc, Canada) as described previously [19, 22]. Briefly, the mice were lightly anesthetized with 2% isoflurane until the heart rate stabilized at 400–500 bpm; then, both conventional two-dimensional images and M-mode images of the heart were acquired in a parasternal short-axis view. Vevo Analysis software was used to calculate LV ejection fraction (LVEF) and LV fractional shortening (LVFS).

Hemodynamic measurement

LV pressures were continuously monitored with a PowerLab system (AD Instrument, Australia) on day 28 after MI as described previously [23]. The LV developed pressure (LVDP), LV end-diastolic pressure (LVEDP), LV maximum ascending rate of pressure ($+dp/dt_{max}$), and LV maximum declining rate of pressure ($-dp/dt_{max}$) were assessed.

Infarct size measurement

The hearts were frozen and cut into 8-μm-thick sections; then, the sections were stained with Modified Masson's Trichrome Stain Kit (Solarbio, China). Infarct size was calculated as the total scar area divided by the LV area, as previously reported [22, 23].

Immunofluorescence

Immunofluorescent staining was performed in the heart tissue sections as previously described [24]. For wheat germ agglutinin (WGA) staining, the sections were stained using an FITC-labeled WGA dye (Sigma-Aldrich). For terminal deoxynucleotidyl transferase dUTP nick end labeling (TUNEL) staining, the sections were stained with an In Situ Cell Death Detection Kit. Cardiomyocytes were identified by the expression of cardiac troponin I (cTnI), and nuclei were counterstained with 4′,6-diamidino-2-phenylindole (DAPI) (Beyotime).

Simultaneous measurement of cell shortening and Ca^{2+} transients

Four weeks after MI or Sham operation, LV cardiomyocytes were isolated from the hearts with a standard enzymatic method as described previously [25] . The collected cardiomyocytes were incubated with a Ca^{2+} indicator (Fura-2 AM) and stimulated electrically by square-wave pulses at a frequency of 0.5 Hz, 1 Hz, and 2 Hz. Ca^{2+} transients and cell shortening were detected simultaneously by a video-based motion edge-detection and Ca^{2+}-recording system (IonOptix) as previously described [25]. Caffeine (10 mmol/L) was applied into normal Tyrode's solution (NT) or the Na^{+}-free and Ca^{2+}-free (0 Na^{+}/0 Ca^{2+}) Tyrode's solution. The amplitude and maximum upstroke velocity (V_{max}) of caffeine-induced Ca^{2+} transients, the rate constants of SERCA-mediated Ca^{2+} transport, and the rate constants of NCX-mediated Ca^{2+} transport were determined as previously described [26].

Ca^{2+}-ATPase activity measurement in cardiac SR

Cardiac SR samples were prepared as described previously [27]. Then, SR Ca^{2+} ATPase activities were determined by measuring inorganic phosphate (Pi)

liberated from ATP hydrolysis and by using Ca^{2+}-pump ATPase Enzyme Assay Kit (Jiancheng Bioengineering Institute, China).

Western blot

Protein extracts were run on sodium dodecyl sulfate polyacrylamide gel electrophoresis (SDS-PAGE) gels in a Protean Electrophoresis Apparatus (Bio-Rad, USA) and then transferred to a polyvinylidene difluoride membrane, as reported previously [25]. The membrane was incubated overnight with primary antibodies against RyR-2 (Sigma-Aldrich), SERCA-2a (Sigma-Aldrich), NCX-1 (Abcam, USA), PLB (Abcam), p-Ser^{16}-PLB (Abcam), p-Thr^{17}-PLB (Santa Cruz, USA), and protein phosphatase 1β (PP-1β) (Proteintech, USA), and was labeled with glyceraldehyde-3-phosphate dehydrogenase (GAPDH) (Proteintech) or β-tubulin (Abcam) antibody to control for unequal loading. Then, the membranes were incubated with horseradish peroxidase (HRP)–conjugated secondary antibodies at room temperature and exposed via enhanced chemiluminescence.

Next-generation sequencing

For exosome samples, preparation of tagged microRNA sequencing libraries, sequencing, and NGS data analysis were performed by LC Sciences (China).

Luciferase reporter assay

The PP-1β sequences containing 127–133 bp were amplified and cloned in pmirGLO dual-luciferase microRNA target expression vector (Promega). The mutant PP-1β 3′UTR pmirGLO vector was generated using QuikChange II XL Site-Directed Mutagenesis Kit (Stratagene, USA) in accordance with the manufacturer's protocol. Next, 293T cells were co-transfected with miR-100-5p mimic and either the PP-1β 3′UTR pmirGLO vector or the mutant PP-1β 3′UTR pmirGLO vector. Then, luciferase activity of the cells was analyzed using a Dual-Glo Luciferase Assay System (Promega). The relative luciferase activity was determined by the ratio of Firefly/Renilla luminescence.

RNA interference

hiPSC-CMs were cultured and transfected with scramble control and PP-1β siRNA (100 nM, RiboBio) by using Lipofectamine $RNAi_{MAX}$ (Thermo Fisher Scientific) in line with the manufacturer's protocols.

RNA isolation and real-time quantitative polymerase chain reaction (RT-qPCR)

microRNA was extracted by TRIzol reagent (Thermo Fisher Scientific) in accordance with the manufacturer's protocols. microRNAs were reverse-transcribed with a TaqMan microRNA Reverse Transcription Kit (ABI) and then analyzed by using Bio-Rad SYBR qPCR (Bio-Rad, USA) on ABI-7900 Real-Time PCR Detection System. The relative expression of microRNA was normalized to U6. The relative expression level was calculated using the $2^{-\Delta\Delta Ct}$ method.

Statistics

Data are presented as mean ± SEM. Differences between two mean values were evaluated via Student's *t*-test, and analysis of variance (ANOVA) with the Tukey's post hoc test was used for multiple comparisons. All statistical analyses were performed in Statistical Product and Service Solutions (SPSS) software (version 18.0, SPSS, USA), and $P < 0.05$ was considered statistically significant.

Results

Characterization of hiPSC-EC and hiPSC-EC exosomes

hiPSCs were reprogrammed from human umbilical cord blood mononuclear cells, and then differentiated into hiPSC-ECs via established protocols [28]. Immunofluorescence staining assessments showed that hiPSC-ECs expressed EC-specific (CD31, CD144, and VWF) markers (**Fig. 1A–C**), and fluorescence-activated cell sorting (FACS) of CD31 analysis demonstrated that the achieved purity of hiPSC-ECs was more than 98% (**Fig. 1D**). hiPSC-ECs also exhibited EC properties, including the formation of tube-like structures on Matrigel in the presence of vascular endothelial growth factor (VEGF) (**Fig. 1E**) and uptake of Ac-LDL (**Fig. 1F**). Subsequently, exosomes were extracted from the hiPSC-EC culture medium via centrifuge ultrafiltration and precipitation in polyethylene glycol. Nanoparticle tracking (**Fig. 1G**) and transmission electron microscopy (**Fig. 1H**) analyses indicated that the isolated exosomes were ~100 nm in diameter and had a double membrane–bound, cup-shaped typical shape. Congruously, western blot confirmed that hiPSC-EC exosomes expressed exosome markers Alix, TSG-101, CD63, and CD9 (**Fig. 1I**). Taken together, these results demonstrated that the generated hiPSC-ECs and isolated hiPSC-EC exosomes exhibited typical characteristics.

hiPSC-EC exosomes protect cardiomyocytes from oxygen and glucose deprivation (OGD) injury in vitro

Then, we examined whether hiPSC-EC exosomes possess a protective effect against OGD injury in cardiomyocytes in vitro. Images of PKH26 fluorescence indicated that when hiPSC-CMs were cultured with PKH26-labeled hiPSC-EC exosomes for 24 hours, numerous exosomes were taken up by the cardiomyocytes (**Fig. 2A**). Next, hiPSC-CMs were cultured under normal or OGD condition treated with PBS or hiPSC-EC exosomes for succedent analyses. TUNEL staining demonstrated that apoptosis of cardiomyocytes with hiPSC-EC exosomes treatment was notably lower than that with PBS treatment under OGD injury (**Fig. 2B, C)**. Consistently, hiPSC-EC exosomes treatment markedly alleviated LDH leakage (**Fig. 2D**) and reversed ATP content of cardiomyocytes (**Fig. 2E**) under OGD injury. Furthermore, the amplitude of Ca^{2+} transients (F340/F380) of OGD cardiomyocytes after hiPSC-EC exosomes treatment was significantly elevated compared with that after PBS treatment (**Fig. 2F, G**). Taken together, hiPSC-EC exosomes exhibited a potential to protect cardiomyocytes from OGD injury by impeding apoptosis, promoting cell survival, improving energy metabolism, and maintaining intracellular Ca^{2+} homeostasis.

hiPSC-EC exosomes improve cardiac function and limit adverse remodeling in a murine MI model

We next investigated the therapeutic efficacy of hiPSC-EC exosomes against MI injury in mice. Cardiac function was evaluated via echocardiographic assessments 28 days after MI (**Fig. 3A**). The measurements of LVEF (**Fig. 3B**) and LVFS (**Fig. 3C**) demonstrated visible amelioration in the MI+EC-Exo group compared with the MI group. Cardiac infarct size was evaluated by Masson's trichrome staining 28 days after MI, and histological analysis revealed that the myocardial infarct size was notably attenuated in the MI+EC-Exo group compared with the MI group (**Fig. 3D, E**). Consistently, the hemodynamic measurements demonstrated that LVDP (**Fig. 3F**), LVEDP (**Fig. 3G**), $+dp/dt_{max}$ (**Fig. 3H**), and $-dp/dt_{max}$ (**Fig. 3i**) in MI+EC-Exo animals were obviously improved compared with MI animals. Furthermore, apparent adverse LV remodeling was progressively reversed after hiPSC-EC exosome treatment 28 days post-MI, as evidenced by a reduction of the ratio of heart weight to body weight (**Fig. 3J**) as well as cardiomyocytes size detected by WGA staining (**Fig. 3K, L**). In addition, TUNEL staining analysis demonstrated that $TUNEL^+$ cardiomyocytes in the border zone of the infarcted hearts were significantly eliminated in MI+EC-Exo animals compared with MI animals three days after MI (**Fig. 3M, N**). Taken together, these results demonstrated that hiPSC-EC exosome administration not only ameliorated the deterioration of heart function, but also attenuated the harmful LV remodeling after MI.

hiPSC-EC exosomes improve cardiomyocyte contraction and Ca^{2+} homeostasis after MI

It is well established that disorder of intracellular Ca^{2+} homeostasis, which is characterized by the dramatic decline in Ca^{2+} transients, reduced SR Ca^{2+} content, and impaired Ca^{2+} uptake and extrusion, is one of the most decisive adverse factors from failing hearts [29]. Thus, we further examined whether hiPSC-EC exosome treatment could rescue these abnormalities. Compared with the Sham group, LV cardiomyocytes isolated from animals of the MI group showed a significant decrease in the ratio of cell shortening amplitude to cell resting length at 1 Hz and 2 Hz. However, this decrease was dramatically rescued in the MI+EC-Exo group (**Fig. 4A, B**). Similar results were observed in the ratio of maximum upstroke velocity of cell shortening ($+dL/dt_{max}$) to cell resting length after hiPSC-EC exosome treatment (**Fig. 4C**). Consistently, the amplitude of Ca^{2+} transients was notably impaired in the MI group at 0.5 Hz, 1 Hz, and 2 Hz stimulation, while these abnormalities were markedly alleviated in the MI+EC-Exo group (**Fig. 4D, E**), which is concordant with the ratio of

maximal ascending rate of Ca^{2+} transients ($+d[Ca^{2+}]/dt_{max}$) to resting Ca^{2+} transients (**Fig. 4F**). Taken together, these results demonstrated that hiPSC-EC exosomes were able to dramatically improve cardiomyocyte contraction and modulate intracellular Ca^{2+} homeostasis in the infarcted hearts.

Effects of hiPSC-EC exosomes on the function of Ca^{2+}-handling proteins in infarcted hearts

Since the disorders of intracellular Ca^{2+} homeostasis could mainly be attributed to the function of critical Ca^{2+}-handling proteins [12, 29-31], we next examined caffeine-induced Ca^{2+} transients from isolated cardiomyocytes after MI to indirectly evaluate the function of main Ca^{2+}-handling proteins (**Fig. 5A**). The markedly reduced caffeine-induced Ca^{2+} transient amplitude with 0 Na^{+}/0 Ca^{2+} Tyrode's solution in the MI group was notably reversed in the MI+EC-Exo group, indicating that hiPSC-EC exosomes were able to enhance the SR Ca^{2+} content (**Fig. 5B**). Subsequently, the rate constant of Ca^{2+} transport by SERCA, which indirectly represents the SERCA function, presented a striking reversal in the MI+EC-Exo group compared with the MI group (**Fig. 5C**). In addition, the V_{max} of caffeine-induced Ca^{2+} transients in 0 Na^{+}/0 Ca^{2+} Tyrode's solution dramatically declined in the MI group, while visible augmentation was confirmed in the MI+EC-Exo group, thereby revealing that hiPSC-EC exosomes could alter the RyR functional abnormality (**Fig. 5D**). However, the rate constant of Ca^{2+} transport by NCX, which indirectly represents the NCX function, showed no apparent differences between the MI+EC-Exo group and the MI group, while it dramatically increased after MI (**Fig. 5E**). Congruously, the measurement of Ca^{2+}-ATPase activity in SR vesicles obtained from the LV tissue revealed that the dramatically declined Ca^{2+}-ATPase activity in the MI group was notably rescued in the MI+EC-Exo group, which indicated the improvement of SERCA function after hiPSC-EC exosome treatment (**Fig. 5F**).

Furthermore, we performed western blot to investigate the influence of hiPSC-EC exosomes on the expression of main Ca^{2+}-handling proteins (**Fig. 6A**). The results revealed that the expression levels of SERCA-2a and RyR-2 were obviously downregulated in the MI group, while these detrimental abnormalities were dramatically diminished in the MI+EC-Exo group (**Fig. 6A, B**). However, no significant difference in NCX-1 protein expression was detected between the MI group and the MI+EC-Exo group (**Fig. 6B**). Subsequently, we evaluated the expression and phosphorylation levels of PLB (**Fig. 6C**), which has been reported to be a major regulator of SERCA-2a [32]. According to the western blot results, the protein expression of PLB and p-thr^{17}-PLB did not show any differences between the MI group and the

MI+EC-Exo group (**Fig. 6D**), while the marked decrease in p-Ser^{16}-PLB in the MI group was apparently reversed in the MI+EC-Exo group (**Fig. 6D**). Taken together, these results demonstrated that hiPSC-EC exosomes were not only able to enhance the protein expression of SERCA-2a, RyR-2, and p-Ser^{16}-PLB, but also rescued the function of SERCA and RyR to maintain cardiomyocyte Ca^{2+} homeostasis after MI.

hiPSC-EC exosome–contained miR-100-5p enhances the phosphorylation of PLB by targeting PP-1β

microRNAs are the dominant active ingredients contained in exosomes and play a key role in cell communication [15, 16, 33]. Therefore, we extracted total RNA in hiPSC-EC exosomes and performed microRNA sequencing. Fifteen microRNAs that were most abundant in hiPSC-EC exosomes were presented (**Fig. 7A**). Considering that miR-100-5p was the most abundant microRNA in hiPSC-EC exosomes and its content was further confirmed by RT-qPCR (**Fig. 7B**), the effect and mechanism of miR-100-5p were further investigated. Through the TargetScan software, we predicated the potential target genes of miR-100-5p and selected PP-1β as a candidate target gene. PP-1β has been reported as one of the catalytic subunits of PP-1, which is the major isotype of serine/threonine phosphatase in cardiomyocytes and plays a pivotal role in regulating the phosphorylation of PLB at Ser^{16} site [34]. Accordingly, luciferase experiment was performed to verify the interaction between PP-1β and miR-100-5p by using a dual-luciferase reporter plasmid containing WT or mutant PP-1β 3' UTR sequence (**Fig. 7C**). Luciferase activity analysis revealed that the luciferase activity in the PP-1β 3' UTR WT under miR-100-5p treatment group was markedly declined, whereas this effect was apparently reversed in the PP-1β 3' UTR mutant with miR-100-5p treatment (**Fig. 7D**). Meanwhile, western blot analysis revealed that the protein expression of PP-1β in the MI+EC-Exo group was dramatically declined compared with that in the MI group (**Fig. 7F**). To further confirm this fine-tuned relationship between PP-1β and PLB, we performed siRNA-mediated gene silencing (**Fig. 7G**). Western blot analysis revealed that the PP-1β expression was notably impaired in the siPP-1β group compared with the scramble group, which presented convincing knockdown efficiency. Importantly, p-Ser^{16}-PLB presented apparent augmentation in the siPP-1β group compared with the scramble group, which indicated the indispensable role of PP-1β in regulating PLB phosphorylation in this model (**Fig. 7H**). Overall, these results demonstrate that PP-1β is the specific downstream gene of miR-100-5p, and that miR-100-5p enriched in hiPSC-EC exosomes enhances the phosphorylation of PLB at Ser^{16} by targeting PP-1β.

miR-100-5p plays an important role in hiPSC-EC exosome–mediated cytoprotection in improving intracellular Ca^{2+} homeostasis and cardiomyocytes survival

To determine the important role of miR-100-5p in hiPSC-EC exosomes–mediated cardio protection, we conducted the miR-100-5p gain–loss function experiments on cardiomyocytes under OGD injury. The western blot analyses revealed that the dramatically declined PP-1β protein expression and elevated p-Ser^{16}-PLB protein level in the OGD+EC-Exo group were abolished in the OGD+EC-$Exo^{anti\text{-}miR\text{-}100\text{-}5p}$ group and reproduced in the OGD+miR-100-5p mimic group (**Fig. 8A, B**). In addition, the notably elevated SERCA activity in the OGD+EC-Exo group was mostly canceled in the OGD+EC-$Exo^{anti\text{-}miR\text{-}100\text{-}5p}$ group and enhanced in the OGD+miR-100-5p mimic group (**Fig. 8C**), which was in line with the change in Ca^{2+} transient amplitude (**Fig. 8D**). Furthermore, miR-100-5p loss partially abrogated while miR-100-5p mimic partially reproduced the effects of hiPSC-EC exosomes on reducing cardiomyocyte apoptosis (**Fig. 8E**) and LDH leakage (**Fig. 8F**). Taken together, these results demonstrate that enriched miR-100-5p contributes to hiPSC-EC exosome–exerted cytoprotective effects on increasing the PLB phosphorylation level and SERCA activity, modulating intracellular Ca^{2+} homeostasis, and promoting cardiomyocytes survival under OGD injury.

Discussion

MI, a cause of congestive heart failure, is a prevalent and staggering health problem with extensive economic burden to society. Therefore, safe and effective treatment options are urgently needed. In this study, we demonstrated the following: (i) In vitro, hiPSC-EC exosomes protected cardiomyocytes from OGD injury by impeding apoptosis, improving energy metabolism, and maintaining intracellular Ca^{2+} homeostasis. (ii) hiPSC-EC exosome administration after MI not only improved the cardiac contractile function, but it also attenuated the harmful LV remodeling. (iii) Mechanistically, hiPSC-EC exosomes strikingly enhanced the function and protein expression of SERCA-2a and RyR-2 to maintain cardiomyocyte Ca^{2+} homeostasis. (iv) miR-100-5p was proven to be the most abundant microRNA, and it was able to elevate the phosphorylation level of PLB at Ser^{16} to improve SERCA-2a activity by targeting PP-1β, thereby contributing to the hiPSC-EC exosome–exerted cytoprotective effects on modulating intracellular Ca^{2+} homeostasis. These findings extend the previous knowledge and provide insights into the mechanisms underlying the cardio protection conferred by hiPSC-EC exosomes, supporting the fact that hiPSC-EC exosomes may be a salutary acellular therapeutic option for MI.

Transplantation of hiPSC-derived endothelial cells combined with other derived cardiac cells has been regarded as a potential therapeutic approach to repair infarcted hearts by recovering cardiac function, limiting adverse fibrosis, suppressing cardiac hypertrophy, diminishing cardiomyocyte apoptosis, and promoting neovascularization [5, 6]. However, low cellular retention and poor engraftment efficacy limit its development [6, 7]. Cumulative evidences have been shown that exosomes generated from transplanted cells, such as adult stem cells, PSCs, and PSC-derived cardiac lineage cells, hold great therapeutic potential for ischemic heart disease [14, 35]. Among them, the recognized therapeutic effect of hiPSC-EC exosomes on ischemic limbs model has paved the way for extending the promising therapeutic potential of hiPSC-EC exosomes to other ischemic diseases, such as ischemic heart disease [36]. Therefore, in this study, we first demonstrated that individual administration of hiPSC-EC exosomes conferred convincing cardioprotective effects, characterized by ameliorating of the heart function worsening, attenuating scar formation, diminishing cardiomyocytes apoptosis, and suppressing cardiac hypertrophy. Our findings raise the possibility that paracrine signaling based on exosomes might be the fundamental mechanism of hiPSC-EC in cardiovascular diseases.

Ca^{2+}, an intracellular ubiquitous second messenger, holds an indispensable role in numerous biological processes, such as muscle contraction, energy metabolism, and cell apoptosis [29, 37]. It has been extensively established that disrupted Ca^{2+} homeostasis (decreased Ca^{2+} transients, reduced SR Ca^{2+} content, increased Ca^{2+} overload) may be considered a critical pathogenic factor in cardiac diseases, including MI-induced HF and atrial fibrillation (AF) [12, 13, 38]. Therefore, it is necessary to maintain intracellular Ca^{2+} homeostasis to alleviate ischemic myocardial injury [12, 13]. Interestingly, we revealed that hiPSC-EC exosomes were able to strikingly enhance the Ca^{2+} transients and cell shortening of cardiomyocytes by elevating the SERCA-2a and RyR-2 function as well as their protein expression, but had no apparent influence on NCX-1 expression and function. Regrettably, the expression and function of L-type calcium channels (LTCC), which enable a small amount of extracellular Ca^{2+} into the cytosol to trigger Ca^{2+} release from SR by RyR-2, and plasma membrane Ca^{2+} ATPase (PMCA) were not evaluated in the present study. Further studies are needed to investigate whether hiPSC-EC exosomes exert influence on these two types of Ca^{2+}-handling proteins. In addition, it is universally acknowledged that systolic function could be enhanced at an increased stimulation frequency under certain physiological conditions. The positive force–frequency relationship (FFR) and calcium–frequency relationship (CaFR) could be considered hallmarks of mature performance of cardiac tissue [6, 39, 40] because the reduction or reversal of the positive FFR, which contributes to contraction abnormality, is observed in human falling hearts [41]. Congruously, in this study, we observed that the amplitude of cell shortening and Ca^{2+} transient as well as $+dL/dt_{max}$/cell resting length and $+d[Ca^{2+}]/dt_{max}$/resting calcium were strikingly rescued by hiPSC-EC exosome administration at a stimulation frequency–dependent manner, which indicated that hiPSC-EC exosomes could rectify the impaired FFR and CaFR of cardiomyocytes from a falling heart.

Increasing intracellular Ca^{2+} level could have implications on energy metabolism and cell apoptosis because the higher Ca^{2+} level needs to be taken up by mitochondria. The disruption of energy supply and utilization balance could further result in stress and apoptotic pathway activation [29]. Meanwhile, the higher intracellular Ca^{2+} level could excessively activate calpain, which is a well-conserved cysteine protease [42]. The hyperactivation of calpain could further degrade cardiac troponin to impair cardiomyocyte contraction and activate multiple cell apoptosis pathways [43]. Congruously, our results revealed the crosstalk between Ca^{2+} homeostasis, energy metabolism, and cell apoptosis mediated by hiPSC-EC exosomes, which could ameliorate the Ca^{2+}

cycling deterioration to further elevate energy metabolism and diminish cardiomyocyte apoptosis. This is also supported by the evidence that gene transfer therapy to rescue SERCA-2a from the falling hearts could restore its energy metabolism to a more efficient state [44]. These findings indicate that Ca^{2+} homeostasis modulation might serve as a molecular mechanism to ameliorate cellular energy metabolism and diminish cardiomyocyte apoptosis.

It is well established that protein function is regulated by a fine equilibrium of protein phosphorylation, which depends on a dynamic balance of protein kinase and phosphatase activities [45]. PP-1, the main abundant serine/threonine phosphatase, plays a pivotal role in regulating protein dephosphorylation and has multiple Ca^{2+}-cycling protein targets such as PLB [34]. A previous study has reported that PP-1β is the major catalytic subunit of PP-1 in the heart that could elevate PLB phosphorylation at Ser^{16} to enhance Ca^{2+} transient and cell shortening [34, 46]. Interestingly, in this study, we linked the inhibition of PP-1β to hiPSC-EC exosome-mediated Ca^{2+} modulation and cardioprotective effects. It is intriguing to observe that hiPSC-EC exosome administration was able to inhibit PP-1β expression in the infarcted myocardium, and that this inhibition further contributed to elevate the phosphorylation of PLB so as to maintain intercellular Ca^{2+} homeostasis. It has been shown that exosomes could be considered therapeutic cargo to communicate between targeted cells and parental cells because exosomes are regarded as the harbor of nonsense oligonucleotides [14-16]. Therefore, another interesting observation is that miR-100-5p, the most abundant microRNA in hiPSC-EC exosomes, may serve as a novel PP-1β inhibitor meditating the PP-1–PLB cascade. Furthermore, gain–loss function analysis demonstrated that miR-100-5p could contribute to hiPSC-EC exosome–provided cytoprotective effects by maintaining intracellular Ca^{2+} homeostasis and abrogating cardiomyocyte apoptosis.

Undoubtedly, there are still some limitations. The present study demonstrated that hiPSC-EC exosome administration was able to eliminate Ca^{2+} homeostasis disorders by rescuing the function and protein expression of SERCA-2a and RyR-2. However, our results only verified that miR-100-5p enriched in hiPSC-EC exosomes could reverse SERCA-2a function through the PP-1β–PLB axis signaling to partially favor cardiomyocyte protection. There is still a need to elucidate the mechanism by which hiPSC-EC exosomes regulate RyR-2 function as well as SERCA-2a and RyR-2 protein expression in future.

Conclusion

Administration of hiPSC-EC exosomes can alleviate ischemic myocardial injury after MI, thereby restoring the heart function and suppressing harmful LV remodeling by modulating resident cardiomyocyte Ca^{2+} homeostasis. Highly enriched miR-100-5p contributes to hiPSC-EC exosome–mediated beneficial effects via the PP-1β–PLB axis signaling.

Abbreviations

hiPSC-ECs: Human induced pluripotent stem cell–derived endothelial cells; MI: myocardial infarction; SERCA-2a: sarcoplasmic reticulum Ca^{2+} ATPase 2a; PLB: phospholamban; PP-1β: protein phosphatase 1β; OGD: oxygen–glucose deprivation; ECM: extracellular matrix; SR: sarcoplasmic reticulum; NCX-1: Na^{+}/Ca^{2+} exchange 1; VWF: von Willebrand factor; Ac-LDL: DiI-conjugated acetylated low-density lipoprotein; Alix: ALG-2-interacting protein X; TSG101: tumor susceptibility gene 101 protein; hiPSC-CMs: hiPSC-derived cardiomyocytes; LDH: lactate dehydrogenase; PBS: phosphate-buffered saline; LAD: left anterior descending artery; LV: left ventricle; LVEF: LV ejection fraction; LVFS: LV fractional shortening; LVDP: LV developed pressure; LVEDP: LV end-diastolic pressure; $+dp/dt_{max}$: LV maximum ascending rate of pressure; $-dp/dt_{max}$: LV maximum declining rate of pressure; WGA: wheat germ agglutinin; TUNEL: terminal deoxynucleotidyl transferase dUTP nick end labeling; cTnI: cardiac troponin I; DAPI: 4′,6-diamidino-2-phenylindole; NT: normal Tyrode's solution; V_{max}: maximum upstroke velocity; ATP: adenosine-triphosphate; SDS-PAGE: sodium dodecyl sulfate polyacrylamide gel electrophoresis; GAPDH: glyceraldehyde-3-phosphate dehydrogenase; RT-qPCR: real-time quantitative polymerase chain reaction; ANOVA: analysis of variance; SPSS: Statistical Product and Service Solutions; FACS: fluorescence-activated cell sorting; VEGF: vascular endothelial growth factor; EC-Exo: endothelial cell–secreted exosomes; WT: wild type; HF: heart failure; AF: atrial fibrillation; LTCC: L-type calcium channel; PMCA: plasma membrane Ca^{2+} ATPase; FFR: positive force–frequency relationship; CaFR: calcium–frequency relationship; BZ: border zone.

Acknowledgments
NA

Author contributions
HL, LW, and LG contributed to the conceptualization and experiment design; HL and LW performed the experiment, collected and analyzed the data; ZML and LG provided funding support; HL and LG contributed to the manuscript writing and final approval manuscript confirmation. All authors have read and approved the final manuscript.

Funding
This work was supported by the National Key Research and Development Program of China (2017YFA0105600, 2020YFA0112600), the National Natural Science Foundation of China (81870208, 82070260), the Shanghai Animal Research Program (21140901800), the Science and Technology Development Fund of Shanghai Pudong New Area (PKJ2020-Y23), and the Peak Disciplines (Type IV) of Institutions of Higher Learning in Shanghai.

Availability of data and materials
Data and materials used and analyzed during the current study are available from the corresponding author upon reasonable request.

Declarations

Ethics approval and consent to participate
All animal procedures and protocols were performed in accordance with the Guide for the Care and Use of Laboratory Animals published by the U.S. National Institutes of Health (8th Edition, 2011) and were approved by the Institutional Animal Care and Use Committee of the Tongji University.

Competing interests
The authors declare that they have no competing interests.

Reference

1. McDonagh TA, Metra M, Adamo M, Gardner RS, Baumbach A, Boehm M, et al. 2021 ESC Guidelines for the diagnosis and treatment of acute and chronic heart failure. European Heart Journal. 2021;42(36):3599-726.

2. Metra M, Teerlink JR. Heart failure. Lancet. 2017;390(10106):1981-95.

3. Cahill TJ, Choudhury RP, Riley PR. Heart regeneration and repair after myocardial infarction: translational opportunities for novel therapeutics. Nature Reviews Drug Discovery. 2017;16(10):699-717.

4. Ziaeian B, Fonarow GC. Epidemiology and aetiology of heart failure. Nature Reviews Cardiology. 2016;13(6):368-78.

5. Ye L, Chang Y-H, Xiong Q, Zhang P, Zhang L, Somasundaram P, et al. Cardiac Repair in a Porcine Model of Acute Myocardial Infarction with Human Induced Pluripotent Stem Cell-Derived Cardiovascular Cells. Cell Stem Cell. 2014;15(6):750-61.

6. Gao L, Gregorich ZR, Zhu W, Mattapally S, Oduk Y, Lou X, et al. Large Cardiac Muscle Patches Engineered From Human Induced-Pluripotent Stem Cell-Derived Cardiac Cells Improve Recovery From Myocardial Infarction in Swine. Circulation. 2018;137(16):1712-+.

7. Gu M, Nguyen PK, Lee AS, Xu D, Hu S, Plews JR, et al. Microfluidic Single-Cell Analysis Shows That Porcine Induced Pluripotent Stem Cell-Derived Endothelial Cells Improve Myocardial Function by Paracrine Activation. Circulation Research. 2012;111(7):882-93.

8. Sahoo S, Adamiak M, Mathiyalagan P, Kenneweg F, Kafert-Kasting S, Thum T. Therapeutic and Diagnostic Translation of Extracellular Vesicles in Cardiovascular Diseases Roadmap to the Clinic. Circulation. 2021;143(14):1426-49.

9. de Abreu RC, Fernandes H, Martins PAdC, Sahoo S, Emanueli C, Ferreira L. Native and bioengineered extracellular vesicles for cardiovascular therapeutics. Nature Reviews Cardiology. 2020;17(11):685-97.

10. Dridi H, Kushnir A, Zalk R, Yuan Q, Melville Z, Marks AR. Intracellular calcium leak in heart failure and atrial fibrillation: a unifying mechanism and therapeutic target. Nature Reviews Cardiology. 2020;17(11):732-47.

11. Zhang H, Makarewich CA, Kubo H, Wang W, Duran JM, Li Y, et al. Hyperphosphorylation of the Cardiac Ryanodine Receptor at Serine 2808 Is

Not Involved in Cardiac Dysfunction After Myocardial Infarction. CircRes. 2012;110(6):831-U87.
12. Zhang Y, Jiao L, Sun LH, Li YR, Gao YQ, Xu CQ, et al. LncRNA ZFAS1 as a SERCA2a Inhibitor to Cause Intracellular Ca2+ Overload and Contractile Dysfunction in a Mouse Model of Myocardial Infarction. CircRes. 2018;122(10):1354-68.
13. Wang R, Wang M, Zhou J, Dai Z, Sun G, Sun X. Calenduloside E suppresses calcium overload by promoting the interaction between L-type calcium channels and Bcl2-associated athanogene 3 to alleviate myocardial ischemia/reperfusion injury. Journal of Advanced Research. 2021;34:173-86.
14. Li Q, Xu Y, Lv K, Wang Y, Zhong Z, Xiao C, et al. Small extracellular vesicles containing miR-486-5p promote angiogenesis after myocardial infarction in mice and nonhuman primates. Science Translational Medicine. 2021;13(584).
15. Hou Z, Qin X, Hu Y, Zhang X, Li G, Wu J, et al. Longterm Exercise-Derived Exosomal miR-342-5p A Novel Exerkine for Cardioprotection. CircRes. 2019;124(9):1386-400.
16. Mayourian J, Ceholski DK, Gorski PA, Mathiyalagan P, Murphy JF, Salazar SI, et al. Exosomal microRNA-21-5p Mediates Mesenchymal Stem Cell Paracrine Effects on Human Cardiac Tissue Contractility. CircRes. 2018;122(7):933-44.
17. Patsch C, Challet-Meylan L, Thoma EC, Urich E, Heckel T, O'Sullivan JF, et al. Generation of vascular endothelial and smooth muscle cells from human pluripotent stem cells. Nat Cell Biol. 2015;17(8):994-1003.
18. Zhang S, Dutton JR, Su L, Zhang J, Ye L. The influence of a spatiotemporal 3D environment on endothelial cell differentiation of human induced pluripotent stem cells. Biomaterials. 2014;35(12):3786-93.
19. Wu Q, Wang J, Tan WLW, Jiang Y, Wang S, Li Q, et al. Extracellular vesicles from human embryonic stem cell-derived cardiovascular progenitor cells promote cardiac infarct healing through reducing cardiomyocyte death and promoting angiogenesis. Cell Death & Disease. 2020;11(5).
20. Gao L, Wang L, Wei Y, Krishnamurthy P, Walcott GP, Menasche P, et al. Exosomes secreted by hiPSC-derived cardiac cells improve recovery from myocardial infarction in swine. Science Translational Medicine. 2020;12(561).

21. Gao L, Zheng Y-J, Gu S-S, Tan J-L, Paul C, Wang Y-G, et al. Degradation of cardiac myosin light chain kinase by matrix metalloproteinase-2 contributes to myocardial contractile dysfunction during ischemia/reperfusion. Journal of Molecular and Cellular Cardiology. 2014;77:102-12.
22. Gao L, Yang L, Wang L, Geng Z, Wei Y, Gourley G, et al. Relationship Between the Efficacy of Cardiac Cell Therapy and the Inhibition of Differentiation of Human iPSC-Derived Nonmyocyte Cardiac Cells Into Myofibroblast-Like Cells. Circ Res. 2018;123(12):1313-25.
23. Wang J, Liu M, Wu Q, Li Q, Gao L, Jiang Y, et al. Human Embryonic Stem Cell-Derived Cardiovascular Progenitors Repair Infarcted Hearts Through Modulation of Macrophages via Activation of Signal Transducer and Activator of Transcription 6. Antioxid Redox Signal. 2019;31(5):369-86.
24. Qiu F, Yuan Y, Luo W, Gong Y-s, Zhang Z-m, Liu Z-m, et al. Asiatic acid alleviates ischemic myocardial injury in mice by modulating mitophagy- and glycophagy-based energy metabolism. Acta Pharmacologica Sinica. 2021.
25. Gao L, Zheng YJ, Gu SS, Tan JL, Paul C, Wang YG, et al. Degradation of cardiac myosin light chain kinase by matrix metalloproteinase-2 contributes to myocardial contractile dysfunction during ischemia/reperfusion. J Mol Cell Cardiol. 2014;77:102-12.
26. Mackiewicz U, Maczewski M, Konior A, Tellez JO, Nowis D, Dobrzynski H, et al. Sarcolemmal Ca2+-ATPase ability to transport Ca2+ gradually diminishes after myocardial infarction in the rat. Cardiovasc Res. 2009;81(3):546-54.
27. Chen Y, Zhao J, Du J, Xu G, Tang C, Geng B. Hydrogen sulfide regulates cardiac sarcoplasmic reticulum Ca(2+) uptake via K(ATP) channel and PI3K/Akt pathway. Life Sci. 2012;91(7-8):271-8.
28. Patsch C, Challet-Meylan L, Thoma EC, Urich E, Heckel T, O'Sullivan JF, et al. Generation of vascular endothelial and smooth muscle cells from human pluripotent stem cells. Nature Cell Biology. 2015;17(8):994-U294.
29. Gorski PA, Ceholski DK, Hajjar RJ. Altered Myocardial Calcium Cycling and Energetics in Heart Failure-A Rational Approach for Disease Treatment. Cell Metabolism. 2015;21(2):183-94.
30. Alvarado FJ, Valdivia HH. Mechanisms of ryanodine receptor 2 dysfunction in heart failure. Nature Reviews Cardiology. 2020;17(11):748-.

31. Hegyi B, Polonen RP, Hellgren KT, Ko CSY, Ginsburg KS, Bossuyt J, et al. Cardiomyocyte Na+ and Ca2+ mishandling drives vicious cycle involving CaMKII, ROS, and ryanodine receptors. Basic Research in Cardiology. 2021;116(1).
32. Kranias EG, Hajjar RJ. Modulation of Cardiac Contractility by the Phopholamban/SERCA2a Regulatome. CircRes. 2012;110(12):1646-60.
33. Liao Z, Chen Y, Duan C, Zhu K, Huang R, Zhao H, et al. Cardiac telocytes inhibit cardiac microvascular endothelial cell apoptosis through exosomal miRNA-21-5p-targeted cdip1 silencing to improve angiogenesis following myocardial infarction. Theranostics. 2021;11(1):268-91.
34. Liu R. Complex functionality of protein phosphatase 1 isoforms in the heart. Cellular Signalling. 2021;85.
35. Khan M, Nickoloff E, Abramova T, Johnson J, Verma SK, Krishnamurthy P, et al. Embryonic Stem Cell-Derived Exosomes Promote Endogenous Repair Mechanisms and Enhance Cardiac Function Following Myocardial Infarction. CircRes. 2015;117(1):52-64.
36. Ye M, Ni Q, Qi H, Qian X, Chen J, Guo X, et al. Exosomes Derived from Human Induced Pluripotent Stem Cells-Endothelia Cells Promotes Postnatal Angiogenesis in Mice Bearing Ischemic Limbs. International Journal of Biological Sciences. 2019;15(1):158-68.
37. Berridge MJ, Lipp P, Bootman MD. The versatility and universality of calcium signalling. Nature Reviews Molecular Cell Biology. 2000;1(1):11-21.
38. Voigt N, Heijman J, Wang Q, Chiang DY, Li N, Karck M, et al. Cellular and Molecular Mechanisms of Atrial Arrhythmogenesis in Patients With Paroxysmal Atrial Fibrillation. Circulation. 2014;129(2):145-56.
39. Ruan JL, Tulloch NL, Razumova MV, Saiget M, Muskheli V, Pabon L, et al. Mechanical Stress Conditioning and Electrical Stimulation Promote Contractility and Force Maturation of Induced Pluripotent Stem Cell-Derived Human Cardiac Tissue. Circulation. 2016;134(20):1557-+.
40. Lamberts RR, Hamdani N, Soekhoe TW, Boontje NM, Zaremba R, Walker LA, et al. Frequency-dependent myofilament Ca2+ desensitization in failing rat myocardium. Journal of Physiology-London. 2007;582(2):695-709.

41. Mulieri LA, Hasenfuss G, Leavitt B, Allen PD, Alpert NR. ALTERED MYOCARDIAL FORCE-FREQUENCY RELATION IN HUMAN HEART-FAILURE. Circulation. 1992;85(5):1743-50.
42. Ono Y, Saido TC, Sorimachi H. Calpain research for drug discovery: challenges and potential. Nature Reviews Drug Discovery. 2016;15(12):854-76.
43. Ke L, Qi XY, Dijkhuis A-J, Chartier D, Nattel S, Henning RH, et al. Calpain mediates cardiac troponin degradation and contractile dysfunction in atrial fibrillation. Journal of Molecular and Cellular Cardiology. 2008;45(5):685-93.
44. Sakata S, Lebeche D, Sakata N, Sakata Y, Chemaly ER, Liang LF, et al. Restoration of mechanical and energetic function in failing aortic-banded rat hearts by gene transfer of calcium cycling proteins. Journal of Molecular and Cellular Cardiology. 2007;42(4):852-61.
45. Nicolaou P, Kranias EG. Role of PP1 in the regulation of Ca cycling in cardiac physiology and pathophysiology. Frontiers in Bioscience-Landmark. 2009;14:3571-84.
46. Aoyama H, Ikeda Y, Miyazaki Y, Yoshimura K, Nishino S, Yamamoto T, et al. Isoform-specific roles of protein phosphatase 1 catalytic subunits in sarcoplasmic reticulum-mediated Ca2+ cycling. Cardiovascular Research. 2011;89(1):79-88.

Figure legends

Figure 1. Characterization of hiPSC-ECs, and exosomes secreted from hiPSC-ECs. (**A–C**) hiPSCs were differentiated into endothelial cells (hiPSC-ECs). hiPSC-ECs were characterized via immunofluorescent analyses of the expression of (**A**) CD31, (**B**) CD144, and (**C**) von Willebrand factor (VWF). Nuclei were counterstained with 4',6-Diamidino-2-Phenylindole (DAPI) (bar = 100 μm). (**D**) Purity of hiPSC-ECs was determined by FACS analysis of CD31. (**E**) hiPSC-ECs were suspended in a culture medium supplemented with 50 ng/mL vascular endothelial growth factor (VEGF) and then plated on Matrigel; 24 hours later, the cells were labeled with calcein, and then tube formation was evaluated under a light microscope (bar = 100 μm). (**F**) The uptake of Dil-conjugated acetylated low-density lipoprotein (Ac-LDL) was evaluated in hiPSC-ECs; nuclei were counterstained with DAPI (bar = 100 μm). (**G–I**) Exosomes were isolated from the culture medium of hiPSC-ECs; then, (**G**) exosome size was evaluated via nanoparticle tracking analysis, (**H**) exosome morphology was evaluated via electron microscopy (bar = 100 nm), and (**I**) the presence of exosome marker proteins (ALG-2-interacting protein X [Alix], tumor susceptibility gene 101 protein [TSG101], CD63, CD9) was evaluated via western blot.

Figure 2. In vitro cytoprotective effects of hiPSC-EC exosomes on hiPSC-CMs. (**A**) hiPSC-derived cardiomyocytes (hiPSC-CMs) were incubated for 24 hours with PKH26-labeled hiPSC-EC exosomes (EC-Exo); then, the cardiomyocytes were fixed and immunofluorescently stained for α-actinin, and nuclei were counterstained with DAPI. Exosomes that had been taken up by the cardiomyocytes were identified by PKH26 fluorescence (bar = 100 μm). (**B–G**) hiPSC-CMs were cultured under normal or oxygen and glucose deprivation (OGD) condition with PBS or hiPSC-EC exosome treatment for 48 hours. (**B**) hiPSC-CMs were fixed, immunofluorescently stained for cardiac troponin I (cTnI) expression and stained by terminal deoxynucleotidyl transferase dUTP nick end labeling (TUNEL); then, nuclei were counterstained with DAPI (bar = 100 μm). (**C**) Quantification for $TUNEL^+$ cardiomyocytes. (**D**) The activity of lactate dehydrogenase (LDH) released in the culture media was measured with a LDH release assay kit. (**E**) hiPSC-CM ATP content was analyzed with an ATP bioluminescence assay kit. (**F-G**) hiPSC-CMs were incubated with a Ca^{2+} indicator (Fura-2 AM); and then Ca^{2+} transients were recorded at 30°C with continuous 0.5 Hz electric stimulation. (**F**) The representative traces of hiPSC-CMs are shown. (**G**) Quantification of Ca^{2+} transient amplitudes. Quantified data are presented as mean ± SEM (n = 4 to 5

independent experiments). Significance was evaluated via Student's *t*-test in (C and D) and one-way ANOVA, followed by Tukey's post hoc test in (E and G). **P*<0.05 and ***P*<0.01.

Figure 3. hiPSC-EC exosomes promote the recovery of cardiac function and limit heart remodeling in a mouse model of myocardial infarction (MI). The mice were divided into the Sham, MI, and MI+EC-Exo groups. (**A–C**) Cardiac function was evaluated on day 28 after MI or Sham surgery via (**A**) echocardiographic assessments. Quantification of (**B**) left ventricular (LV) ejection fraction (LVEF) and (**C**) LV fractional shorting (LVFS). (**D**) Representative images of infarct size after 28 days with Masson trichrome staining. (**E**) Quantitative data of infarct size (%) were calculated by infarct size/total LV areas. (**F–I**) Hemodynamic measurement of (**F**) LV developed pressure (LVDP), (**G**) LV end diastolic pressure (LVEDP), (**H**) LV maximum ascending rate of pressure ($+dp/dt_{max}$), and (**I**) LV maximum declining rate of pressure ($-dp/dt_{max}$) were performed 28 days post-MI. (**J**) Heart to body weight ratio (HW/BW) 28 days after MI. (**K**) Sections from the border zone (BZ) of the infarcted heart (28 days after MI) were stained with wheat germ agglutinin (WGA) to identify the cellular borders, and with cTnI to visualize CMs; nuclei were counterstained with DAPI (bar = 100 μm); then, (**L**) cardiomyocyte cross-sectional surface areas were measured. (**M**) The sections obtained from the border zone (3 days post-MI) were stained with antibodies against cTnI, apoptotic cells were identified via a TUNEL staining, and nuclei were counterstained with DAPI (bar = 100 μm); then, (**N**) apoptosis was quantified as the percentage of $TUNEL^+$ cells. Quantified data are presented as mean ± SEM. n = 9–11 per experimental group in (B, C, and F–J) and n = 5–6 per experimental group in (E, L, and N). Significance was evaluated via Student's *t*-test in (E) and one-way ANOVA followed by Tukey's post hoc test in (B, C, and F-J, L, N). **P*<0.05 and ***P*<0.01.

Figure 4. Cell shortening and calcium transient assessments in isolated cardiomyocytes after MI. The rod-shaped cardiomyocytes were isolated from mouse left ventricles of the Sham group, MI group, and MI+EC-Exo group on day 28 after MI or Sham surgery. Cardiomyocytes were incubated with a Ca^{2+} indicator (Fura-2 AM); then, cell shortening and Ca^{2+} transients were recorded at 30°C under continuous 0.5 Hz, 1 Hz, and 2 Hz electric stimulation. (**A**) Representative traces of cell shortening. Quantification of (**B**) amplitude of cell shortening/cell resting length and (**C**) maximum upstroke velocity of cell shortening ($+dL/dt_{max}$)/cell resting length. (**D**) Representative traces of calcium transients. Quantification of (**E**) amplitude of Ca^{2+} transient and (**F**) maximal

ascending rate in cell contractile Ca^{2+} transients (+d[Ca^{2+}]/dt_{max})/resting calcium. Quantified data are presented as mean ± SEM. A total of 40–44 cardiomyocytes from four different hearts were measured in each group. Significance was evaluated via one-way ANOVA, followed by Tukey's post hoc test in (B, C, E, and F). ***P*<0.01.

Figure 5. Sarcoplasmic reticulum (SR) Ca^{2+} content and Ca^{2+} transport rate assessments in isolated cardiomyocytes after MI. Ca^{2+} transients were evoked by 10 mM caffeine in ventricular myocytes from the Sham group, MI group, and MI+EC-Exo group on day 28 after MI or Sham surgery. (**A**) Representative traces of Ca^{2+} transient during caffeine-induced contraction in 0 Na^+/0 Ca^{2+} Tyrode's solution or normal Na^+/Ca^{2+} Tyrode's solution (NT). (**B**) Quantification of the amplitude of caffeine-induced Ca^{2+} transients in 0 Na^+/0 Ca^{2+} Tyrode's solution. (**C**) Rate constant of SERCA-mediated Ca^{2+} transport (the difference between rate constant of caffeine-evoked Ca^{2+} transients and electric stimulation-evoked Ca^{2+} transients in NT solution). (**D**) Maximum upstroke velocity (V_{max}) of caffeine-induced Ca^{2+} transient in 0 Na^+/0 Ca^{2+} Tyrode's solution. (**E**) Rate constant of Na^+/Ca^{2+} exchanger-1 (NCX-1)-mediated Ca^{2+} transport (the difference between delay rate constant of caffeine-evoked Ca^{2+} transients in NT solution and in 0 Na^+/0 Ca^{2+} solution). (**F**) SERCA activity was accessed by a Ca^{2+}-pump ATPase enzyme assay kit. Quantified data are presented as mean ± SEM. A total of 40–44 cardiomyocytes from four different hearts were measured per group in (B–E) and n = 5–6 per experimental group in (F). Significance was evaluated via one-way ANOVA, followed by Tukey's post hoc test in (B–F). ***P*<0.01.

Figure 6. Evaluation of calcium-handling protein expression. Protein samples of heart tissues were collected from different groups 28 days post-MI or Sham surgery. (**A–B**) Western blot to assess the expression levels of calcium-handling proteins, including ryanodine receptor 2 (RyR-2), NCX-1, and SERCA-2a. (**A**) Representative immunoblots. (**B**) Quantified analysis of protein expression. (**C–D**) Western blot to assess the protein expression levels of phospholamban (PLB), p-Ser^{16}-PLB, and p-Thr^{17}-PLB. (**C**) Representative immunoblots. (**D**) Quantified analysis of protein expression levels. Quantified data are presented as mean ± SEM, n = 4–5 in each group. Significance was evaluated via one-way ANOVA, followed by Tukey's post hoc test in (B and D). **P*<0.05 and ***P*<0.01.

Figure 7. PP-1β is the direct target of miR-100-5p. (**A**) Total RNA was extracted from hiPSC-EC exosomes, and microRNA sequencing was

performed. The expression of the 15 microRNAs that were most abundant are displayed in a bar graph; data are expressed as log_2 of exosomal microRNA normalized read counts. (**B**) microRNA quantity of miR-100-5p in human dermal fibroblast exosomes (FB-Exo) and hiPSC-EC exosomes (EC-Exo) were measured via RT-qPCR and normalized to measurements in hiPSC-EC exosomes. (**C–D**) Luciferase activity analysis to investigate the miR-100-5p target gene, serine/threonine specific protein phosphatase 1 catalytic subunits β (PP-1β). (**C**) Wild-type or mutant dual-luciferase reporter plasmid was constructed according to the predicted binding sequence in 3' UTR of PP-1β or mutant sequence and then (**D**) the activities of renilla and firefly luciferase were determined with the Dual Luciferase Reporter Assay system. (**E–F**) Western blot was performed to assess the PP-1β protein expression in heart tissues 28 days post-MI or Sham surgery. (**E**) Representative immunoblots. (**F**) Quantified protein expression. (**G-H**) siPP-1β and scramble control were transfected into hiPSC-CMs to confirm gene-silencing efficiency and downstream gene regulation. (**G**) Representative immunoblots. (**H**) Quantified protein expression. Quantified data are presented as mean ± SEM, n = 4–5 independent experiments. Significance was evaluated via one-way ANOVA, followed by Tukey's post hoc test in (D, F, and H) and Student's *t*-test in (B). $^{**}P<0.01$

Figure 8. miR-100-5p loss abolishes while miR-100-5p mimic reproduces the part of protection of hiPSC-EC exosomes on cardiomyocyte against OGD injury. hiPSC-CMs were separately treated with PBS, mimic negative control (NC), miR-100-5p mimic, EC-Exo, EC-Exo^{NC}, and EC-Exo$^{anti\text{-}miR\text{-}100\text{-}5p}$ under OGD condition. (**A–B**) Protein samples were collected from the above-mentioned groups, and then western blot was performed to access the protein expression levels of PP-1β, p-Ser16-PLB, and PLB. (**A**) Representative immunoblots. (**B**) Quantified analysis of protein expression levels. (**C**) SERCA activity was assessed by a Ca^{2+}-pump ATPase enzyme assay kit. (**D**) hiPSC-CMs were incubated with a Ca^{2+} indicator (Fura-2 AM) and stimulated under 0.5 Hz; then, Ca^{2+} transients were recorded and quantified. (**E**) The activity of LDH released in the culture media was measured. (**F**) TUNEL^{+} cardiomyocytes were assessed. Quantified data are presented as mean ± SEM, n = 4–5 independent experiments. Significance was evaluated via one-way ANOVA, followed by Tukey's post hoc test in (B–F). $^{*}P<0.05$ and $^{**}P<0.01$.

Figures

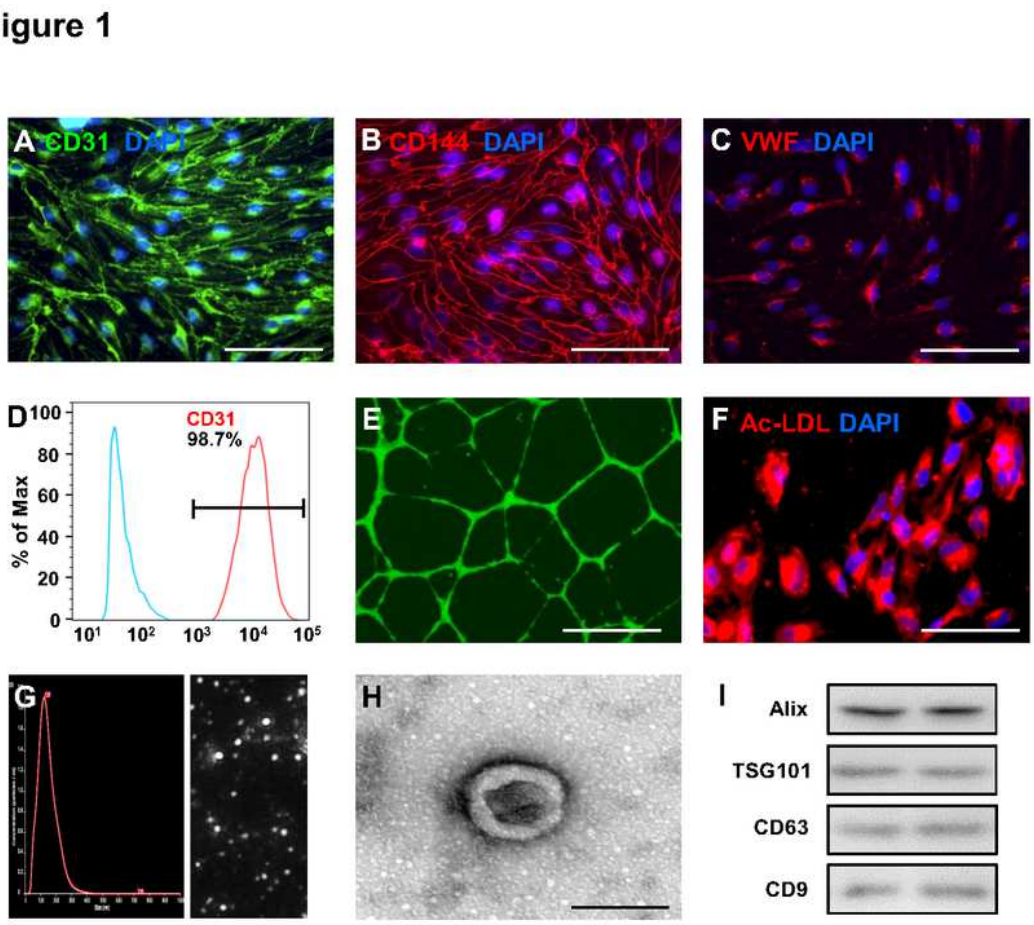

Figure 1

Characterization of hiPSC-ECs, and exosomes secreted from hiPSC-ECs. (A–C) hiPSCs were differentiated into endothelial cells (hiPSC-ECs). hiPSC-ECs were characterized via immunofluorescent analyses of the expression of (A) CD31, (B) CD144, and (C) von Willebrand factor (VWF). Nuclei were

counterstained with 4',6-Diamidino-2-Phenylindole (DAPI) (bar = 100 μm). (D) Purity of hiPSC-ECs was determined by FACS analysis of CD31. (E) hiPSC-ECs were suspended in a culture medium supplemented with 50 ng/mL vascular endothelial growth factor (VEGF) and then plated on Matrigel; 24 hours later, the cells were labeled with calcein, and then tube formation was evaluated under a light microscope (bar = 100 μm). (F) The uptake of Dil-conjugated acetylated low-density lipoprotein (Ac-LDL) was evaluated in hiPSC-ECs; nuclei were counterstained with DAPI (bar = 100 μm). (G–I) Exosomes were isolated from the culture medium of hiPSC-ECs; then, (G) exosome size was evaluated via nanoparticle tracking analysis, (H) exosome morphology was evaluated via electron microscopy (bar = 100 nm), and (I) the presence of exosome marker proteins (ALG-2-interacting protein X [Alix], tumor susceptibility gene 101 protein [TSG101], CD63, CD9) was evaluated via western blot.

Figure 2

Figure 2

In vitro cytoprotective effects of hiPSC-EC exosomes on hiPSC-CMs. (A) hiPSC-derived cardiomyocytes (hiPSC-CMs) were incubated for 24 hours with PKH26-labeled hiPSC-EC exosomes (EC-Exo); then, the cardiomyocytes were fixed and immunofluorescently stained for α-actinin, and nuclei were counterstained with DAPI. Exosomes that had been taken up by the cardiomyocytes were identified by PKH26 fluorescence (bar = 100 μm). (B–G) hiPSC-CMs were cultured under normal or oxygen and glucose

deprivation (OGD) condition with PBS or hiPSC-EC exosome treatment for 48 hours. (B) hiPSC-CMs were fixed, immunofluorescently stained for cardiac troponin I (cTnI) expression and stained by terminal deoxynucleotidyl transferase dUTP nick end labeling (TUNEL); then, nuclei were counterstained with DAPI (bar = 100 μm). (C) Quantification for TUNEL+ cardiomyocytes. (D) The activity of lactate dehydrogenase (LDH) released in the culture media was measured with a LDH release assay kit. (E) hiPSC-CM ATP content was analyzed with an ATP bioluminescence assay kit. (F-G) hiPSC-CMs were incubated with a Ca2+ indicator (Fura-2 AM); and then Ca2+ transients were recorded at 30°C with continuous 0.5 Hz electric stimulation. (F) The representative traces of hiPSC-CMs are shown. (G) Quantification of Ca2+ transient amplitudes. Quantified data are presented as mean ± SEM (n = 4 to 5 independent experiments). Significance was evaluated via Student's t-test in (C and D) and one-way ANOVA, followed by Tukey's post hoc test in (E and G). *P<0.05 and **P<0.01.

Figure 3

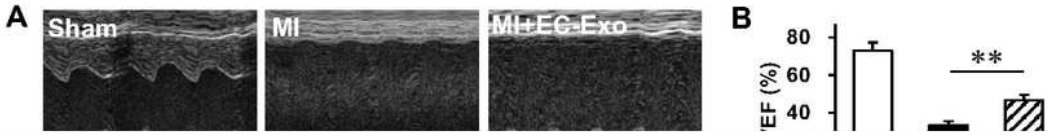

Figure 3

hiPSC-EC exosomes promote the recovery of cardiac function and limit heart remodeling in a mouse model of myocardial infarction (MI). The mice were divided into the Sham, MI, and MI+EC-Exo groups. (A–C) Cardiac function was evaluated on day 28 after MI or Sham surgery via (A) echocardiographic assessments. Quantification of (B) left ventricular (LV) ejection fraction (LVEF) and (C) LV fractional shorting (LVFS). (D) Representative images of infarct size after 28 days with Masson trichrome staining.

(E) Quantitative data of infarct size (%) were calculated by infarct size/total LV areas. (F–I) Hemodynamic measurement of (F) LV developed pressure (LVDP), (G) LV end diastolic pressure (LVEDP), (H) LV maximum ascending rate of pressure (+dp/dtmax), and (I) LV maximum declining rate of pressure (-dp/dtmax) were performed 28 days post-MI. (J) Heart to body weight ratio (HW/BW) 28 days after MI. (K) Sections from the border zone (BZ) of the infarcted heart (28 days after MI) were stained with wheat germ agglutinin (WGA) to identify the cellular borders, and with cTnI to visualize CMs; nuclei were counterstained with DAPI (bar = 100 μm); then, (L) cardiomyocyte cross-sectional surface areas were measured. (M) The sections obtained from the border zone (3 days post-MI) were stained with antibodies against cTnI, apoptotic cells were identified via a TUNEL staining, and nuclei were counterstained with DAPI (bar = 100 μm); then, (N) apoptosis was quantified as the percentage of TUNEL+ cells. Quantified data are presented as mean ± SEM. n = 9–11 per experimental group in (B, C, and F–J) and n = 5–6 per experimental group in (E, L, and N). Significance was evaluated via Student's t-test in (E) and one-way ANOVA followed by Tukey's post hoc test in (B, C, and F-J, L, N). *P<0.05 and **P<0.01.

Figure 4

Cell shortening and calcium transient assessments in isolated cardiomyocytes after MI. The rod-shaped cardiomyocytes were isolated from mouse left ventricles of the Sham group, MI group, and MI+EC-Exo group on day 28 after MI or Sham surgery. Cardiomyocytes were incubated with a Ca2+ indicator (Fura-2 AM); then, cell shortening and Ca2+ transients were recorded at 30°C under continuous 0.5 Hz, 1 Hz, and 2 Hz electric stimulation. (A) Representative traces of cell shortening. Quantification of (B) amplitude of cell shortening/cell resting length and (C) maximum upstroke velocity of cell shortening (+dL/dtmax)/cell resting length. (D) Representative traces of calcium transients. Quantification of (E) amplitude of Ca2+ transient and (F) maximal 28 ascending rate in cell contractile Ca2+ transients (+d[Ca2+]/dtmax)/resting calcium. Quantified data are presented as mean ± SEM. A total of 40–44 cardiomyocytes from four different hearts were measured in each group. Significance was evaluated via one-way ANOVA, followed by Tukey's post hoc test in (B, C, E, and F). **P<0.01.

Figure 5

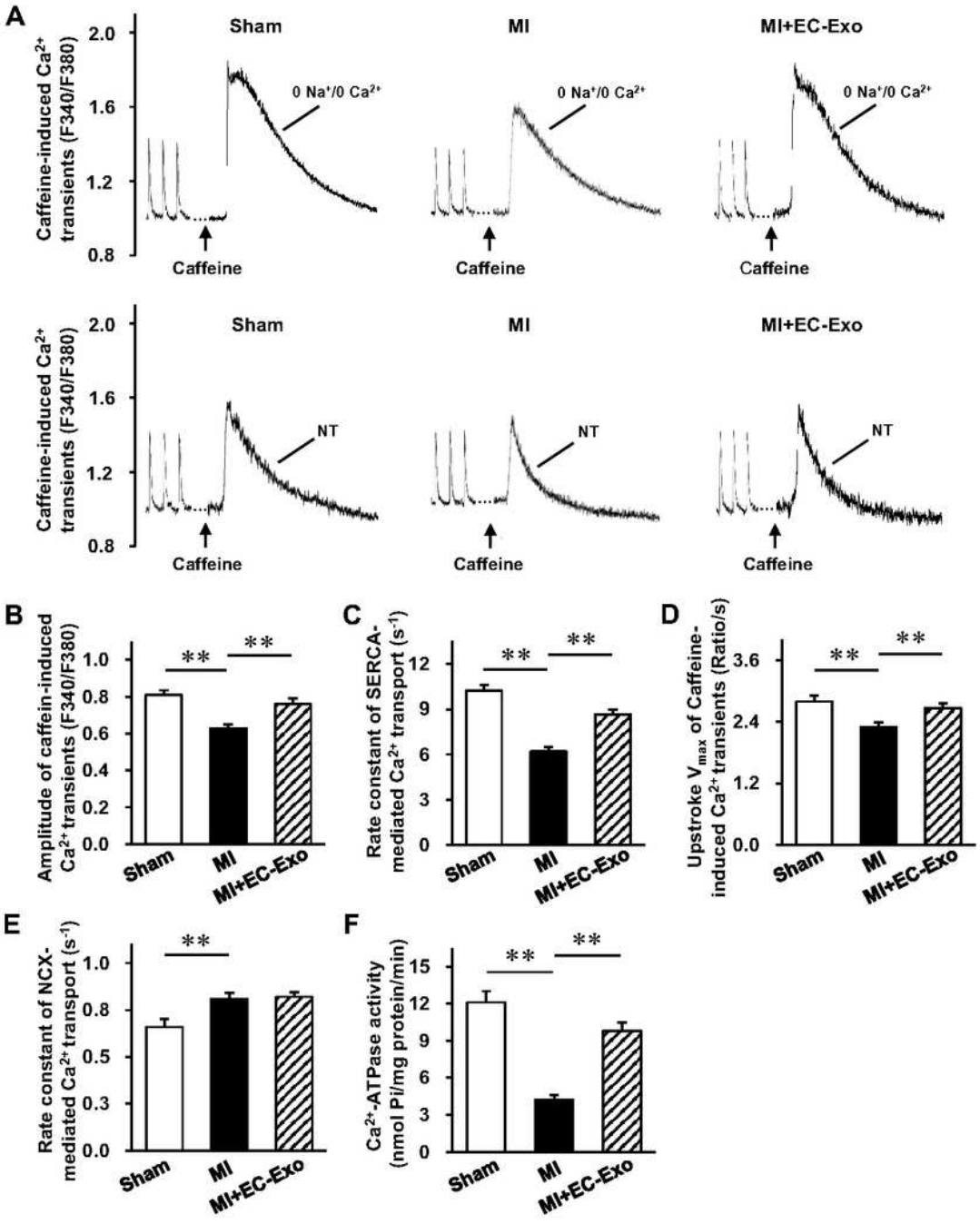

Figure 5

Sarcoplasmic reticulum (SR) Ca2+ content and Ca2+ transport rate assessments in isolated cardiomyocytes after MI. Ca2+ transients were evoked by 10 mM caffeine in ventricular myocytes from the Sham group, MI group, and MI+EC-Exo group on day 28 after MI or Sham surgery. (A) Representative traces of Ca2+ transient during caffeine-induced contraction in 0 Na+ /0 Ca2+ Tyrode's solution or normal Na+ /Ca2+ Tyrode's solution (NT). (B) Quantification of the amplitude of caffeine-induced Ca2+

transients in 0 Na+ /0 Ca2+ Tyrode's solution. (C) Rate constant of SERCA-mediated Ca2+ transport (the difference between rate constant of caffeine-evoked Ca2+ transients and electric stimulation-evoked Ca2+ transients in NT solution). (D) Maximum upstroke velocity (Vmax) of caffeine-induced Ca2+ transient in 0 Na+ /0 Ca2+ Tyrode's solution. (E) Rate constant of Na+ /Ca2+ exchanger-1 (NCX-1)-mediated Ca2+ transport (the difference between delay rate constant of caffeine-evoked Ca2+ transients in NT solution and in 0 Na+ /0 Ca2+ solution). (F) SERCA activity was accessed by a Ca2+ -pump ATPase enzyme assay kit. Quantified data are presented as mean ± SEM. A total of 40–44 cardiomyocytes from four different hearts were measured per group in (B–E) and n = 5–6 per experimental group in (F). Significance was evaluated via one-way ANOVA, followed by Tukey's post hoc test in (B–F). **P<0.01.

Figure 6

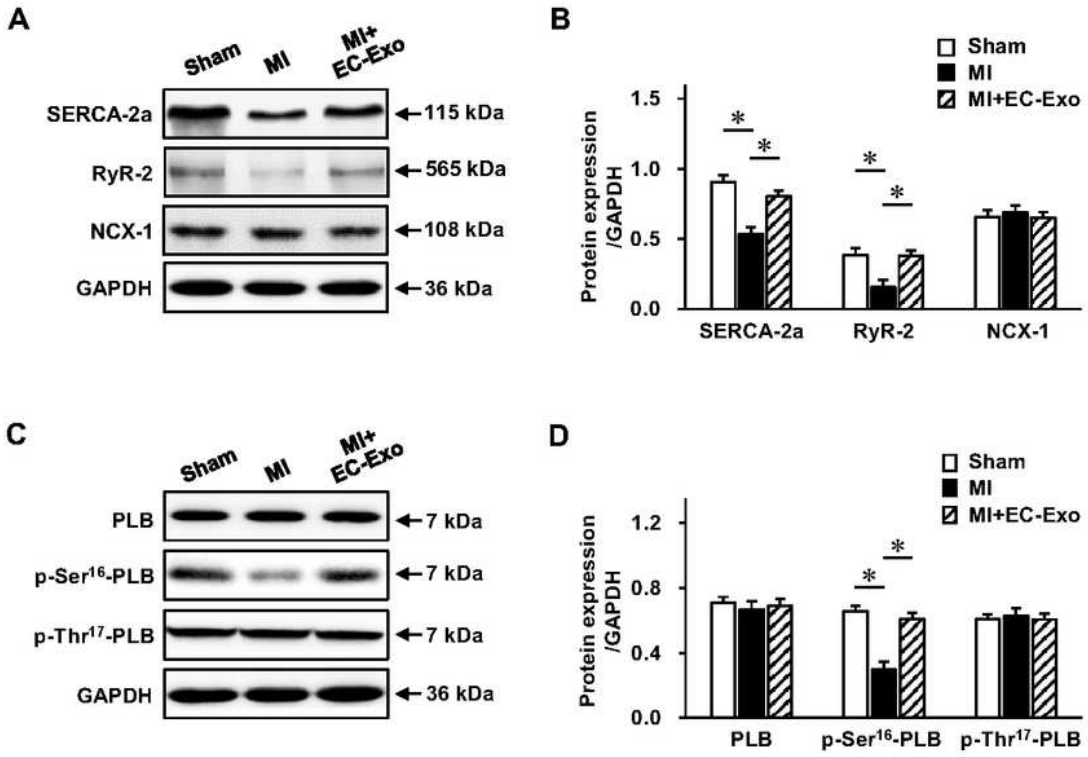

Figure 6

Evaluation of calcium-handling protein expression. Protein samples of heart tissues were collected from different groups 28 days post-MI or Sham surgery. (A–B) Western blot to assess the expression levels of calcium-handling proteins, including ryanodine receptor 2 (RyR-2), NCX-1, and SERCA-2a. (A) Representative immunoblots. (B) Quantified analysis of protein expression. (C–D) Western blot to assess the protein expression levels of phospholamban (PLB), p-Ser16 -PLB, and p-Thr17 -PLB. (C)

Representative immunoblots. (D) Quantified analysis of protein expression levels. Quantified data are presented as mean ± SEM, n = 4–5 in each group. Significance was evaluated via one-way ANOVA, followed by Tukey's post hoc test in (B and D). *P<0.05 and **P<0.01.

Figure 7

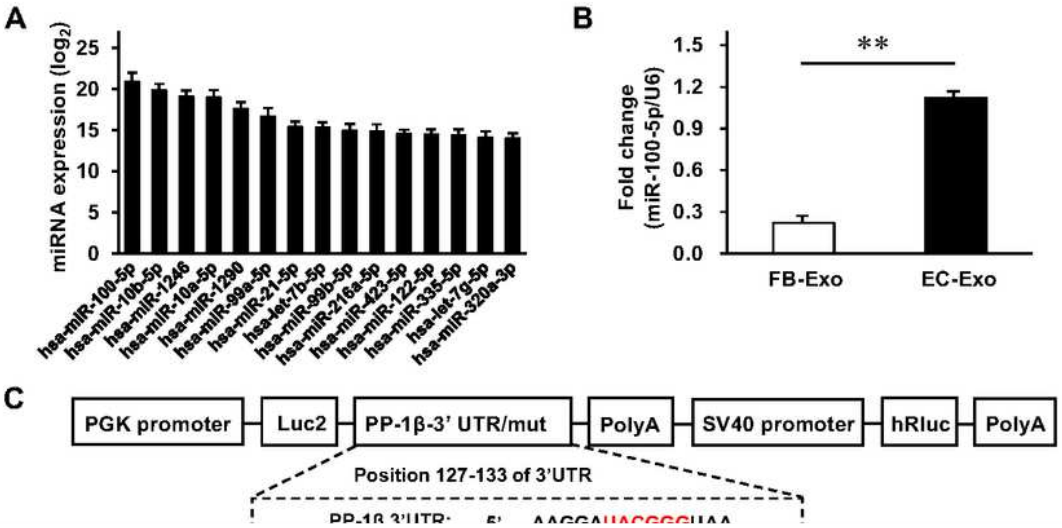

Figure 7

PP-1β is the direct target of miR-100-5p. (A) Total RNA was extracted from hiPSC-EC exosomes, and microRNA sequencing was performed. The expression of the 15 microRNAs that were most abundant are displayed in a bar graph; data are expressed as log2 of exosomal microRNA normalized read counts. (B) microRNA quantity of miR-100-5p in human dermal fibroblast exosomes (FB-Exo) and hiPSC-EC exosomes (EC-Exo) were measured via RT-qPCR and normalized to measurements in hiPSC-EC exosomes. (C–D) Luciferase activity analysis to investigate the miR-100-5p target gene, serine/threonine specific protein phosphatase 1 catalytic subunits β (PP-1β). (C) Wild-type or mutant dual-luciferase reporter plasmid was constructed according to the predicted binding sequence in 3' UTR of PP-1β or mutant sequence and then (D) the activities of renilla and firefly luciferase were determined with the Dual Luciferase Reporter Assay system. (E–F) Western blot was performed to assess the PP-1β protein expression in heart tissues 28 days post-MI or Sham surgery. (E) Representative immunoblots. (F) Quantified protein expression. (G-H) siPP-1β and scramble control were transfected into hiPSC-CMs to confirm gene-silencing efficiency and downstream gene regulation. (G) Representative immunoblots. (H) Quantified protein expression. Quantified data are presented as mean ± SEM, n = 4–5 independent experiments. Significance was evaluated via one-way ANOVA, followed by Tukey's post hoc test in (D, F, and H) and Student's t-test in (B). **P<0.01

Figure 8

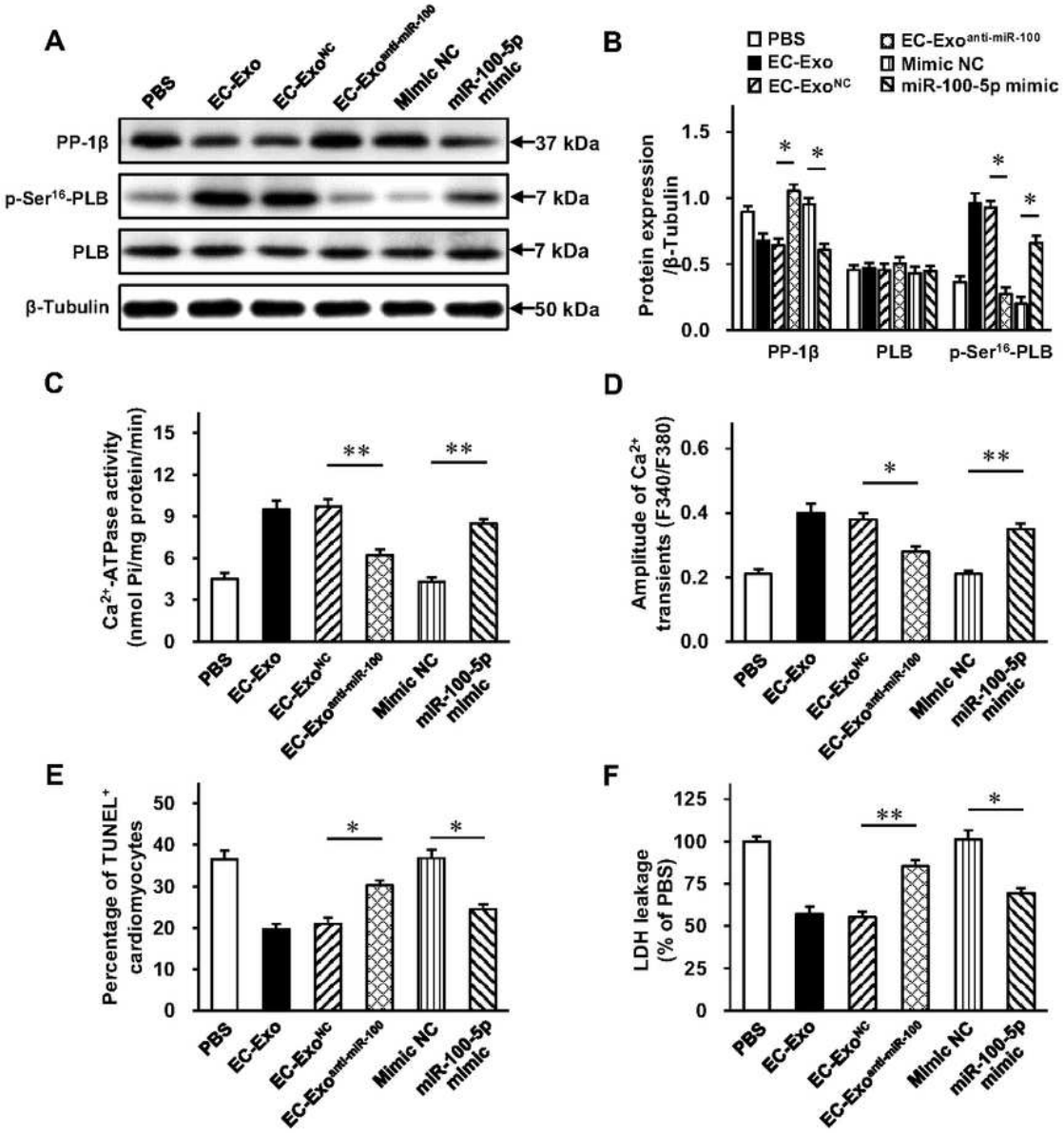

Figure 8

miR-100-5p loss abolishes while miR-100-5p mimic reproduces the part of protection of hiPSC-EC exosomes on cardiomyocyte against OGD injury. hiPSC-CMs were separately treated with PBS, mimic negative control (NC), miR-100-5p mimic, EC-Exo, EC-ExoNC, and EC-Exoanti-miR-100-5p under OGD condition. (A–B) Protein samples were collected from the above-mentioned groups, and then western blot was performed to access the protein expression levels of PP-1β, p-Ser16-PLB, and PLB. (A)

Representative immunoblots. (B) Quantified analysis of protein expression levels. (C) SERCA activity was assessed by a Ca2+ -pump ATPase enzyme assay kit. (D) hiPSC-CMs were incubated with a Ca2+ indicator (Fura-2 AM) and stimulated under 0.5 Hz; then, Ca2+ transients were recorded and quantified. (E) The activity of LDH released in the culture media was measured. (F) TUNEL+ cardiomyocytes were assessed. Quantified data are presented as mean ± SEM, n = 4–5 independent experiments. Significance was evaluated via one-way ANOVA, followed by Tukey's post hoc test in (B–F). *P<0.05 and **P<0.01.